Transition pathway of CO2 crystals under high pressures

AUTHOR(S):

Togo, Atsushi; Oba, Fumiyasu; Tanaka, Isao

CITATION:

Togo, Atsushi ...[et al]. Transition pathway of CO2 crystals under high pressures. PHYSICAL REVIEW B 2008, 77(18): 184101.

ISSUE DATE:

2008-05

URL:

http://hdl.handle.net/2433/84636

PHYSICAL REVIEW B **77**, 184101 (2008)

Transition pathway of CO_2 crystals under high pressures

Atsushi Togo,[1,*] Fumiyasu Oba,[1] and Isao Tanaka[1,2]
[1]*Department of Materials Science and Engineering, Kyoto University, Sakyo, Kyoto 606-8501, Japan*
[2]*Nanostructures Research Laboratory, Japan Fine Ceramics Center, Atsuta, Nagoya 456-8587, Japan*
(Received 4 March 2008; revised manuscript received 6 April 2008; published 1 May 2008)

The pressure-induced transitions from molecular to nonmolecular CO_2 crystals are systematically investigated by using first-principles lattice dynamics calculations. Geometrically, likely transition pathways are derived from the dynamical instability of the molecular crystals under high pressures. Layered CO_2 crystals composed of a two-dimensional network of corner-sharing CO_4 tetrahedra are proposed as metastable products of high-pressure phases obtained through the transition pathways. The layered crystals are similar to phase VI in geometry and Raman spectrum.

DOI: 10.1103/PhysRevB.77.184101 PACS number(s): 61.43.Bn, 63.20.D−, 64.70.K−

I. INTRODUCTION

While CO_2 exists in the gas phase as an important component of the Earth's atmosphere, it forms a variety of crystals at high pressures.[1–17] The aggregation of CO_2 molecules is known to form molecular CO_2 crystals, preserving the strong C-O double bond.[5–8,12,13,15–18] Three phases denoted by II,[5,7,8] III,[8,12,13,15–17] and IV (Refs. 5, 6, 8, 12, 16, and 18) have been produced by applying high pressure and high temperature to phase I (*dry ice*). Applying further compression and heat brings about the nonmolecular structures, which are denoted by phase V.[4,10,11] The formation of amorphous CO_2 (Ref. 3) (a-CO_2) and phase VI (Ref. 1) is also reported by the compression of phases III and II, respectively. Although the structures of these high-pressure phases have been investigated by Raman spectroscopy and synchrotron x-ray powder diffraction, they have not been unambiguously determined. Theoretical calculations of the high-pressure CO_2 phases have also been reported by a few groups.[19–23] Enthalpy differences among many nonmolecular polymorphs composed of CO_4 tetrahedra are small,[19] which is analogous to SiO_2 crystals. Although β-cristobalite-type CO_2 was reported to be the most stable structure over a wide range of high pressures, experiments indicate the presence of other structures.[19] This is suggestive of the presence of metastable structures that can be formed during the compression experiments.

In this paper, we present possible transition pathways leading to nonmolecular CO_2 crystals at high pressures, determined by using first-principles lattice dynamics calculations. The transition pathways and compression products are obtained through the analysis of vibration modes that induce structural instability and therefore spontaneous phase transition under applied pressure.

II. METHODS

The first-principles calculations were performed in the framework of density functional theory within the generalized gradient approximation[24] and using the plane-wave projector augmented wave (PAW) method[25] as implemented in the VASP code.[26–28] We employed the PAW data sets for C and O with a radial cutoff of 0.58 Å and a plane-wave energy cutoff of 900 eV. The Brillouin zone sampling and convergence criteria for the energy and geometry of the phases were carefully determined to be sufficient to discuss the phase transition and enthalpy differences. The transition pathways and the structures of the high-pressure phases were determined as follows. First, the structure was optimized using a conjugate-gradient algorithm under various applied pressures. The internal forces and stresses were converged within 10^{-6} eV/Å and 5×10^{-3} GPa, respectively. Phonon calculations were then performed for the optimized structures. When an imaginary mode was found, the crystal symmetry was partially lowered by the atomic displacements corresponding to the eigenvector of the imaginary mode. Further geometry optimization with the lowered symmetry resulted in a spontaneous structural transformation as expected from the presence of the imaginary mode. The phonon calculations were performed by the frozen phonon method as implemented in the FROPHO code[29] developed by the present authors. The force constants were derived from forces calculated by the PAW method in a supercell with a small atomic displacement of 0.01 Å. Supercells with at least 16 CO_2 molecular units were used.

III. RESULTS AND DISCUSSION

We have chosen phases II ($P4_2/mnm$), III ($Cmce$), and two types of phase IV, i.e., IVa ($Pbcn$) and IVb ($P4_12_12$), as starting crystals according to experimental results in the literature. Phase I is excluded since it transforms to phases II–IV by compression.[5–8,12,13,15–18] The CO_2 stacking patterns in phases II, III, and IVa can be differentiated by their topological carbon sites. The structure of phase IVb is similar to that of phase II except that the unit cell size in the c axis doubles that of phase II and the CO_2 molecular units are bent and slightly tilted.[6] Phases II–IV have been classified into different categories depending on the literature. In the present study, they are included in the category of molecular crystals since the structure of each CO_2 unit in these crystals optimized in the present study is nearly identical to that of the CO_2 molecule.

The predicted transition pathways and compression products are summarized in Fig. 1. We define the transition pathway as a tentative crystal structure related to the starting

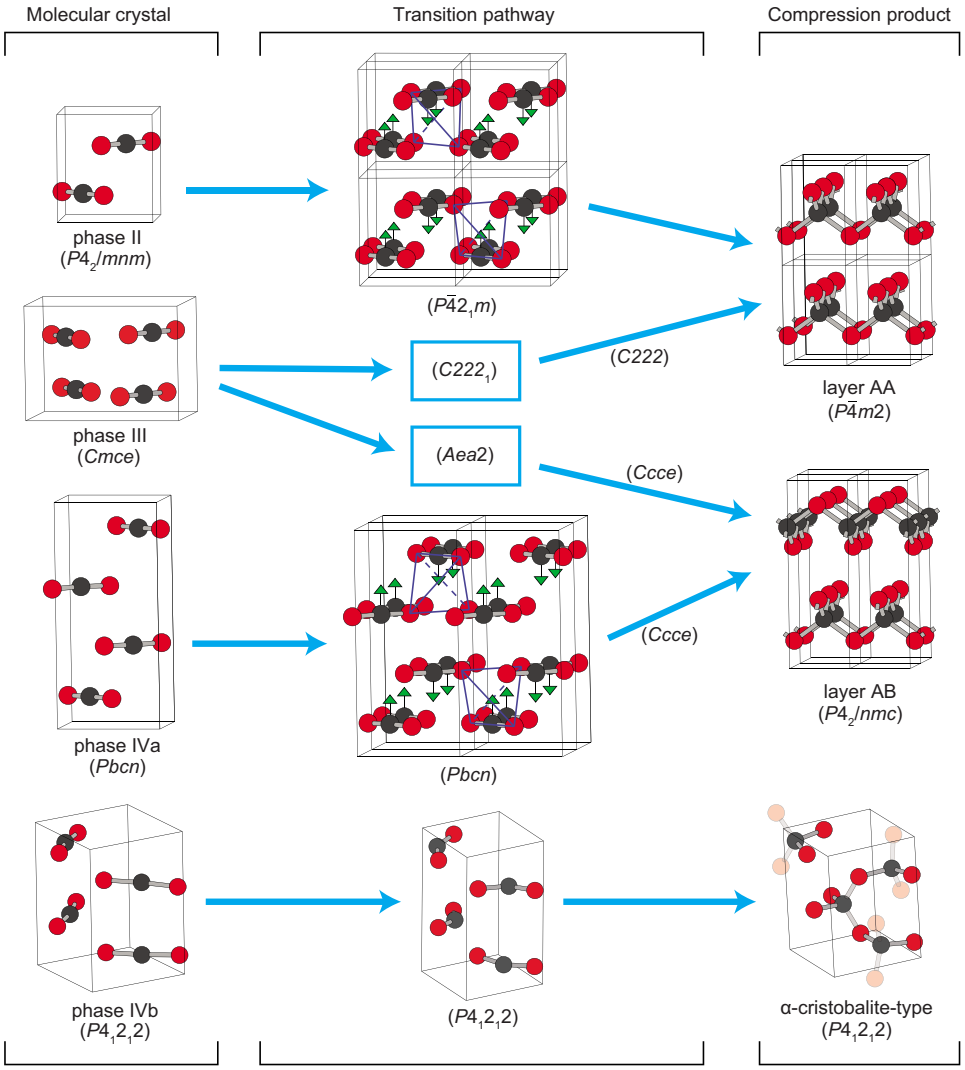

FIG. 1. (Color online) Predicted phase relationships in the molecular to nonmolecular transitions of CO_2. The black and red circles denote carbon and oxygen atoms, respectively. The space groups of the molecular and nonmolecular phases and those on the transition pathways are shown in the parentheses.

molecular crystal and the compression product in symmetry. When the double bond starts to break, the symmetry becomes lower than, or equivalent to, that of the starting molecular crystal, as shown in the left and middle columns. Here, we assume that the symmetry lowering is only allowed when an imaginary mode, which represents the dynamical instability of the crystal structure, arises. In most cases, the imaginary modes obtained from the molecular crystals were found at the Γ point or the Brillouin zone boundary. During the bond reconstruction toward the compression product, the symmetry is heightened, or is kept unchanged, as shown in the middle and right columns. The symmetry heightening is determined by spontaneous atomic relaxation under the symmetry constraints of the crystal structure. As a consequence, the compression products shown in the right panel of Fig. 1 are obtained, which are confirmed to be dynamically stable using lattice dynamics calculations. The space groups of the various crystal structures represent the crystallographical relationships. For example, phase II ($P4_2/mnm$) shows the transition to layer AA ($P\bar{4}m2$) along the pathway whose space group is denoted by $P\bar{4}2_1m$. $P\bar{4}2_1m$ is a subgroup of both $P4_2/mnm$ and $P\bar{4}m2$.

In addition to the α-cristobalite-type phase, we found two types of layered crystals composed of a two-dimensional network of corner-sharing CO_4 tetrahedra as compression products, which are named here as layers AA and AB according to their stacking sequences. Layer AA is composed of $AAAA\cdots$ stacking, whereas layer AB shows alternating $ABAB\cdots$ stacking, where A and B layers are the same in structure and face different orientations that are 90° with respect to each other. A structure analogous to layer AB was theoretically reported as a compression product of phase III.[23] No reports can be found for a structure analogous to layer AA. The relationship in crystal structure between layer AA and the starting crystal, phase II, is presented in Fig. 1. The arrows in the middle panel indicate the atomic displacements corresponding to the imaginary mode that appears at ~130 GPa under the constraints of the $P4_2/mnm$ symmetry. Phase II is transferred to a structure on the transition pathway by involving the small atomic displacements. On the pathway, the carbon atoms freely relax until they sit at the center of the tetrahedra, which is enclosed by the blue lines. Layer AA with CO_4 tetrahedra is thus formed.

Layer AB is the compression product of phase IVa. Previous experimental studies have proposed that phase IVa can consist of bent CO_2,[6] while another study has indicated the linearity of CO_2.[5] First-principles calculations have suggested linear CO_2 up to 50 GPa.[21] In our results, phase IVa is

also composed of nearly linear CO_2 at 0 GPa. However, with increasing pressure, the CO_2 molecular unit gradually and slightly bends. For example, the O-C-O angle is ~177° at 60 GPa. The arrows in the middle panel of Fig. 1 indicate the orientations of relaxation of the carbon atoms. At ~110 GPa, the structure overcomes the potential barrier and transforms to layer *AB*. The tetrahedron depicted by the blue lines corresponds to one of the CO_4 tetrahedra in layer *AB*.

In contrast to the simple geometric relationships of these two systems, phase III to layer *AA* and to layer *AB* transitions are geometrically not simple since relative shifts of molecular layers in a plane parallel to the layers are required in both cases. Under the constraints of the *Cmce* symmetry, two individual imaginary modes appear at ~180 and ~190 GPa. The induced transition pathways have space groups of $Aea2$ and $C222_1$, respectively, resulting in the transition to layer *AB* and layer *AA*, respectively. Another layered structure is obtained from phase III. At ~180 GPa, a phonon band on the Brillouin zone path between the points $\Gamma(0,0,0)$ and $V(0,0,\pi/c)$ becomes imaginary under the constraints of the *Cmce* symmetry. After relaxing the crystal along the imaginary mode at the *V* point, the layered structure denoted by *AABBAABB*··· stacking appears. From imaginary modes of other points between the two points, other stacking structures that have longer periodicity may be obtained.

Phase IVb transforms to the α-cristobalite-type phase at above ~90 GPa. The structure of phase IVb depicted in Fig. 1 is based on experimentally determined atomic coordinates,[6] which gives slightly bent molecular CO_2. Below ~80 GPa, our calculations indicated that this structure is energetically unfavorable and the unit cell of phase IVb is spontaneously reduced to two phase II unit cells with linear CO_2 by geometry optimization. Above ~90 GPa, it transforms into the α-cristobalite-type phase. Thus, phase IVb with nonlinear CO_2 was not found in the present study. As shown in Fig. 1, the structure of the compression product, the α-cristobalite-type phase, is easily correlated to that of the starting phase IVb and the tentative structure on the transition pathway.

C-O bond lengths and C-O-C angles of layers *AA* and *AB* at 60 GPa are very close with each other, 1.38 Å and 108°–110°, respectively. The CO_4 tetrahedra of these phases are close to regular tetrahedra. In contrast, that of the α-cristobalite-type phase is distorted a little. The C-O bond lengths are 1.34 and 1.37 Å, and the C-O-C angles are 107°–118°.

In Fig. 2, the computed relative enthalpies of layer *AA*, layer *AB*, and the α-cristobalite-type phase are compared to the molecular phases and some candidate nonmolecular structures given in Ref. 19 as a function of pressure. The enthalpy differences are calculated relative to the β-cristobalite-type phase, which is found to show the lowest enthalpy among the nonmolecular structures. Although layers *AA* and *AB* exhibit lower enthalpy than the molecular phases II to IV above ~40 GPa, the enthalpies are still several hundred meV higher than that of the β-cristobalite-type phase. The α-cristobalite-type phase becomes more favorable than the molecular phases above ~25 GPa and has ~200 meV higher enthalpy than the β-cristobalite-type phase. Layers

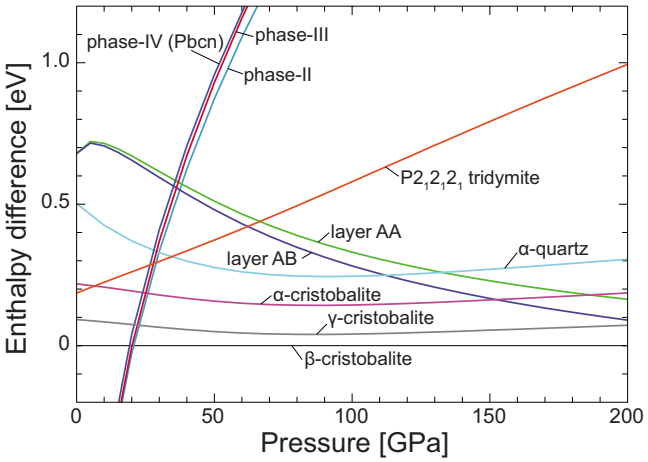

FIG. 2. (Color online) Enthalpy differences relative to the β-cristobalite-type phase as a function of pressure. The enthalpy difference is normalized by a CO_2 molecular unit.

AA, *AB*, and the α-cristobalite-type phase are therefore metastable. Layers *AA* and *AB* are composed of a two-dimensional network of tetrahedra, which are far different from the other nonmolecular phases, which have a three-dimensional network of tetrahedra. The metastable layered structures may therefore not easily transform into more stable phases such as the β-cristobalite-type phase once they are formed. On the other hand, it is expected that the α-cristobalite-type phase will hardly maintain its metastable state and will transform immediately into the β-cristobalite-type phase under the established experimental condition since these two structures are intimately related.[30]

The calculated Raman modes for layers *AA*, *AB*, and the β-cristobalite-type phase are compared to the experimental results for phases V and VI (Ref. 1) in Fig. 3. The Raman modes for phase VI at ~600 and ~900 cm^{-1} are close to the intralayer vibrational modes of layer *AA* (layer *AB*) as denoted by E (E_g) and A_1 (A_{1g}), respectively. However, correspondence is not found for the modes at ~300 and ~1100 cm^{-1}. To identify major Raman-active modes, the Raman intensity was calculated in the framework of density functional perturbation theory implemented in the QUANTUM-ESPRESSO package.[31] As a result, the peaks at ~600 and ~900 cm^{-1} are found to be much stronger than the other peaks. The Raman mode for phase V located at ~750 cm^{-1} is close to that of the β-cristobalite-type phase as denoted by A_1, which confirms the findings reported by Dong *et al.*[20]

The analogy in the major vibrational modes between the layered structures and phase VI is attributed to the similarity in atomic arrangement. In both structures, the carbon atoms move significantly at the transition from phase II, while the oxygen sublattice remains almost unchanged. Layer *AA* is regarded as the case where the disordered carbon atoms in phase VI are aligned on one side in the O_6 octahedra. Simulated x-ray powder diffraction patterns of layers *AA* and *AB* at 60 GPa are shown in Fig. 4. The x-ray wavelength of 0.3682 Å was employed to compare to experimental patterns of phase VI given in Fig. 5(a) of Ref. 1. The reported patterns of phase VI are characterized by one strong peak at ~10° and very weak peaks spread over the given range of

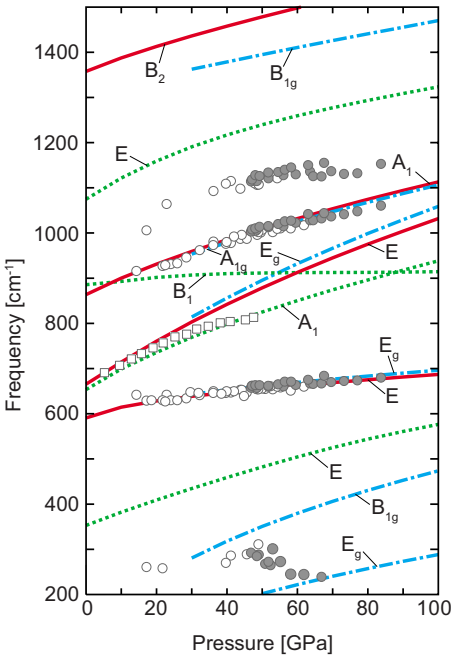

FIG. 3. (Color online) Calculated Raman modes of layer *AA* (solid line), layer *AB* (dotted-dashed line), and the β-cristobalite-type phase (dotted line) and experimentally obtained modes[1] (symbols) as a function of pressure. The circle and square symbols are assigned to the phases VI and V reported in Ref. 1, respectively. The open and filled symbols indicate the data obtained with increasing and decreasing pressures, respectively. The theoretical frequencies are rescaled by +4% to compare with the experimental results. The Raman modes of the β-cristobalite-type phase are selected in the same way as in Ref. 20.

6°–20°. As expected from the above-mentioned analogies in the local structure, the simulated patterns of both layers *AA* and *AB* also show one strong peak. However, the peak position is ~1° higher than that of phase VI [Fig. 5(a) of Ref. 1]. Since interaction between the layers is weak in the layered structures, distance between layers can be readily affected by external conditions, e.g., temperature effect. Since 1° deviation is too large to attribute to thermal expansion effects, we consider that the disorder plays an important role to expand the distance between layers. If the disorder is not so high, the diffraction peaks of {*hk*0} possibly agree with the experimental patterns better than those of {*hkl*} due to the strong binding between tetrahedra in the *a*-*b* plane. In addition to the discrepancy in the position of the main peak, the other peaks are clearer and the number of peaks is smaller in layers *AA* and *AB* than in phase VI. This is presumably due to the ordered structures in layers *AA* and *AB*.

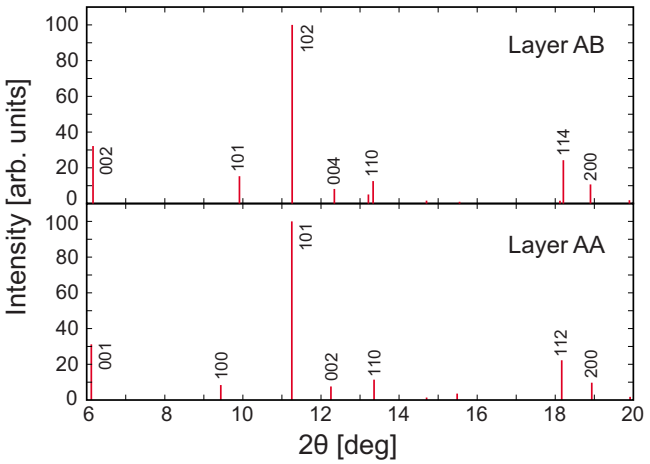

FIG. 4. (Color online) Simulated x-ray powder diffraction patterns of layers *AA* and *AB* at 60 GPa. The numbers along with representative intensities are Miller indices.

An analogous behavior between phase VI and the predicted layered structures also seems to exist in the transition pathway. Phase VI has been obtained both from phases II and III (Ref. 1) as we found two pathways to layer *AA* from phases II and III. Our results indicate that the transition pathway of phase II to layer *AA* is more straightforward than that of phase III to layer *AA* from the geometric viewpoint. This can explain the experimental observation of less crystalline phase VI produced from phase III.[1]

IV. SUMMARY

We have performed systematic first-principles lattice dynamics calculations to predict possible transition pathways leading to nonmolecular CO_2 crystals at high pressures. Through the transition pathways determined by the dynamical instability of molecular CO_2 crystals, layered structures and α-cristobalite-type structure are obtained as metastable products of high-pressure phases. We propose that the layered structures composed of a two-dimensional network of corner-sharing CO_4 tetrahedra are similar to phase VI in geometry and Raman spectrum. Our results provide insights into the molecular to nonmolecular transition and metastable compression products of CO_2.

ACKNOWLEDGMENTS

This work was supported by three programs from the Ministry of Education, Culture, Sports, Science and Technology of Japan, i.e., the Grants-in-Aid for Scientific Research (A), Priority Area on “atomic scale modification” (No. 474), and the global COE program.

*togo.atsushi@gmail.com

[1] V. Iota, C. S. Yoo, J. H. Klepeis, Z. Jenei, W. Evans, and H. Cynn, Nat. Mater. **6**, 34 (2007).
[2] M. Santoro and F. A. Gorelli, Chem. Soc. Rev. **35**, 918 (2006).
[3] M. Santoro, F. A. Gorelli, R. Bini, G. Ruocco, S. Scandolo, and W. A. Crichton, Nature (London) **441**, 857 (2006).
[4] M. Santoro, J. F. Lin, H. K. Mao, and R. J. Hemley, J. Chem. Phys. **121**, 2780 (2004).
[5] F. A. Gorelli, V. M. Giordano, P. R. Salvi, and R. Bini, Phys. Rev. Lett. **93**, 205503 (2004).

[6] J. H. Park, C. S. Yoo, V. Iota, H. Cynn, M. F. Nicol, and T. Le Bihan, Phys. Rev. B **68**, 014107 (2003).
[7] C. S. Yoo, H. Kohlmann, H. Cynn, M. F. Nicol, V. Iota, and T. LeBihan, Phys. Rev. B **65**, 104103 (2002).
[8] V. Iota and C. S. Yoo, Phys. Rev. Lett. **86**, 5922 (2001).
[9] O. Tschauner, H. K. Mao, and R. J. Hemley, Phys. Rev. Lett. **87**, 075701 (2001).
[10] C. S. Yoo, H. Cynn, F. Gygi, G. Galli, V. Iota, M. Nicol, S. Carlson, D. Hausermann, and C. Mailhiot, Phys. Rev. Lett. **83**, 5527 (1999).
[11] V. Iota, C. S. Yoo, and H. Cynn, Science **283**, 1510 (1999).
[12] H. Olijnyk and A. P. Jephcoat, Phys. Rev. B **57**, 879 (1998).
[13] R. Lu and A. M. Hofmeister, Phys. Rev. B **52**, 3985 (1995).
[14] K. Aoki, H. Yamawaki, M. Sakashita, Y. Gotoh, and K. Takemura, Science **263**, 356 (1994).
[15] K. Aoki, H. Yamawaki, and M. Sakashita, Phys. Rev. B **48**, 9231 (1993).
[16] H. Olijnyk, H. Däufer, H. J. Jodl, and H. D. Hochheimer, J. Chem. Phys. **88**, 4204 (1988).
[17] R. C. Hanson, J. Phys. Chem. **89**, 4499 (1985).
[18] C. S. Yoo, V. Iota, and H. Cynn, Phys. Rev. Lett. **86**, 444 (2001).
[19] J. Dong, J. K. Tomfohr, O. F. Sankey, K. Leinenweber, M. Somayazulu, and P. F. McMillan, Phys. Rev. B **62**, 14685 (2000).
[20] J. Dong, J. K. Tomfohr, and O. F. Sankey, Phys. Rev. B **61**, 5967 (2000).
[21] S. A. Bonev, F. Gygi, T. Ogitsu, and G. Galli, Phys. Rev. Lett. **91**, 065501 (2003).
[22] B. Holm, R. Ahuja, A. Belonoshko, and B. Johansson, Phys. Rev. Lett. **85**, 1258 (2000).
[23] S. Serra, C. Cavazzoni, G. L. Chiarotti, S. Scandolo, and E. Tosatti, Science **284**, 788 (1999).
[24] J. P. Perdew, K. Burke, and M. Ernzerhof, Phys. Rev. Lett. **77**, 3865 (1996).
[25] P. E. Blöchl, Phys. Rev. B **50**, 17953 (1994).
[26] G. Kresse, J. Non-Cryst. Solids **193**, 222 (1995).
[27] G. Kresse and J. Furthmüller, Comput. Mater. Sci. **6**, 15 (1996).
[28] G. Kresse and D. Joubert, Phys. Rev. B **59**, 1758 (1999).
[29] A. Togo, http://fropho.sourceforge.net
[30] E. Bourova, S. C. Parker, and P. Richet, Phys. Rev. B **62**, 12052 (2000).
[31] S. Baroni *et al.*, http://www.pwscf.org/